Progress In Electromagnetics Research M, Vol. 67, 177–188, 2018

Automated Scaling Region of Interest with Iterative Edge Preserving in Forward-Backward Time-Stepping

Juliana Nawawi[1], Shafrida Sahrani[2, *], and Kismet Anak Hong Ping[2]

Abstract—A one-shot rescaling process, namely Automated Scaling Region of Interest (AS-ROI), is combined with an inversion technique of Forward-Backward Time-Stepping (FBTS). The purpose is to alleviate the ill-posedness and nonlinearity of inverse problem by reducing the size of the unknown problem. The inversion solution is carried out to reconstruct tumour as an unknown object in coarse investigation domain of lung area which is then rescaled down corresponding to object location and size. In this paper, edge preserving methods consisting of edge preserving regularization and anisotropic diffusion are imposed alternately on the solution and reconstructed profiles to improve the current method of AS-ROI. Results on the reconstructed lungs and tumours give significant insight of the proposed work. Accuracy level for the reconstructed profiles are significantly improved in spite that spatial resolution is retained as the original setting of FBTS.

1. INTRODUCTION

Inverse scattering to solve unknown problems can be unravelled with deterministic [1–3] or stochastic [4–6] inversion solutions. The solution can be formulated either in frequency or time-domain. Findings from several research works in frequency domain of inversion technique with monochromatic source have shown quite satisfying outcomes [7, 8]. The approach has been proven less complex and faster in computation [7]. It also eliminates the needs to compute wave path which is ill-posed to solve [9]. Main limitation of frequency domain implementation is inadequacies of data that can be acquired. In [10], the number of transmitters utilized was up to 128 nodes for single and multi-frequency cases to acquire more data, in which parallel solution was proposed to compensate the computational burden. Apart from that, the implementation in frequency domain approach would be complicated in effort to overcome diffraction limit by reducing the size of wavelength or using high frequency [11].

Multi-frequency technique is commonly proposed to acquire more information on sought object to be characterized as discussed in [12]. Therefore, formulation of inversion solution in time-domain is preferred due to diversity in frequencies that can be exploited. However, common drawback of time inversion technique is the expense of computational despite its potential benefits in image reconstruction. FBTS is a deterministic inversion technique which is implemented in time domain. By exploiting broad range of frequencies to acquire fields scattered by the object in many iterations, the implementation is surely expensive in computation. This problem motivates researchers to improve the conventional method into an effective solution.

Iterative multi-scaling approach (IMSA) is widely applied to increase the precision details of reconstructed images [13, 14]. Segmentation concept in IMSA [1, 15, 16] to extract object location was adapted into AS-ROI method to define new and fine reconstruction region. Innovative aspect of this research work lies in the number of steps required to extract the object's area. In contrast to IMSA,

Received 30 January 2018, Accepted 18 March 2018, Scheduled 17 April 2018
* Corresponding author: Shafrida Sahrani (sshafrida@unimas.my).
[1] Department of Electrical Engineering, Polytechnic Kuching Sarawak, Malaysia. [2] Applied Electromagnetics Research Group, Department of Electrical & Electronics Engineering, Faculty of Engineering, Universiti Malaysia Sarawak, Malaysia.

AS-ROI only requires single iteration of inversion technique to define the new reconstruction region that corresponds to size, shape and location of the detected object. Resolution degree is maintained throughout the optimization process which is unlike IMSA that uses multi-resolution technique. The implementation of AS-ROI in FBTS can be considered to abide the efficacy criteria stated in [17], which is a non-complex in algorithm, has reasonably number of parameters and is anticipated to assist the optimization reaching optimal convergence.

This paper presents a comprehensive study of paper [18] which has been extended to be a regularized version of combined AS-ROI and FBTS. Regularized case in this research work refers to a combined method of AS-ROI and edge preserving techniques in FBTS. Regularization often offers promising outcomes in stabilizing inversion solution [19, 20]. The notion of iterative spatial filtering imposed on the reconstructed profiles was also integrated into the solution [21]. Most research studies related to FBTS have been applied to breast imaging with either real-like phantom breast model [22–26] or simple objects taken after breast profiles [19–21, 27]. Therefore, the proposed method was analysed against intrinsic problem of inverse scattering to reconstruct tumour in lung profiles' distribution in this research work. Similar to a previous study in [18], only relative permittivity was considered for reconstruction region segmentation. Therefore, results for this study only report the accuracy of reconstructed relative permittivity profiles.

2. METHOD

2.1. Automated Scaling Region of Interest (AS-ROI) in Forward-Backward Time-Stepping (FBTS)

Configuration of problem geometry is illustrated as in Figure 1. Lossy and homogeneous objects are considered for analyses under an ideal situation in which scattered fields are not affected by noise. In this research framework, lung area is considered as the original reconstruction region, and a tumour of 8 mm in radius is the object to seek. Both lung and tumour are embedded in a free space medium to allow perfect signal propagation. The lung is surrounded by $\mathbf{M = 12}$ point source antennas. Each point source antenna is positioned with the same distance at $\mathbf{r^t_m(m = 12, \ldots, M)}$ in a radial formation. Only one antenna can transmit modulated Gaussian pulse signal based impressed current formulated as in Eq. (1) towards the region of interest (ROI) at a time.

$$J_Z^m(rt) = I(t)\delta(r - r_m^t) \quad r = [x, y] \tag{1}$$

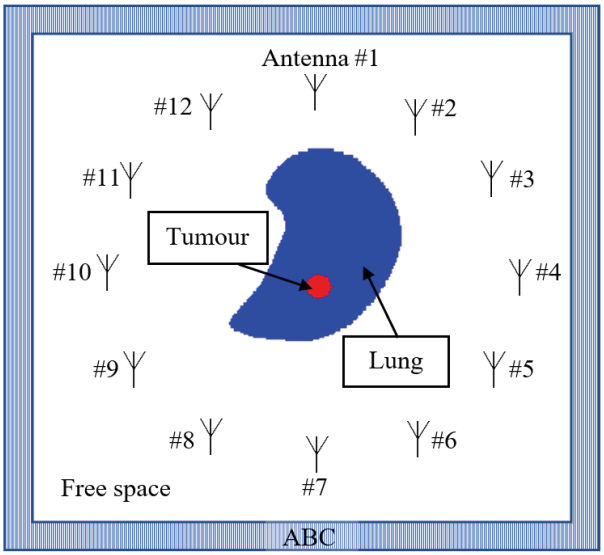

Figure 1. Configuration of problem geometry.

J_Z^m in Eq. (1) is the line current source pointing to z-direction, r the spatial position, t the time, $I(t)$ a sinusoidal current, and $\delta(r)$ the Dirac function. The remaining antennas act as receivers to collect total scattered fields from the ROI. Number of receivers is denoted as $N(N = M - 1)$ located at $r_n^r(n = 1, 2, \ldots, N)$. The fields measurement process therefore shall generate a total scattered fields dataset of $M \times N$ equivalent to 132 dataset.

FBTS is solved by means of optimization utilizing conjugate gradient based method of Polak-Ribière-Polyak directions in which cost function is minimized. On condition that cost function is minimized or has reached the convergence, reconstructed object profiles must be approximate to the actual model in which size, shape and location of sought object can be estimated, provided by a suitable value of the initial guess. The cost function of optimization is expressed in Eq. (2).

$$F(\rho) = \int_0^T \sum_{m=1}^{M} \sum_{n=1}^{N} K_{mn}(t) \left|\nu_m\left(\rho\left(r\right); r_n^r, t\right) - \tilde{\nu}_m\left(r_n^r, t\right)\right|^2 dt \tag{2}$$

$$\rho = [\varepsilon_r(r), \sigma(r)] \quad r = [x, y] \tag{3}$$

Forward Time-Stepping is implemented to obtain the total fields scattered by actual object in the initial ROI, namely measured scattered fields $\tilde{\nu}_m\left(r_n^r, t\right)$. The same process is repeated at each iteration of optimization to collect the total scattered fields of estimated object. These collected fields due to estimated profiles are referred as calculated scattered fields $\nu_m\left(\rho\left(r\right); r_n^r, t\right)$. Parameter $K_{mn}(t)$ is a nonnegative weighting function which becomes zero at time $t = T$, in which T is the total measurement period. The term ρ given in Eq. (3) refers to dielectric profiles, involving relative permittivity $\varepsilon_r(r)$ and conductivity $\sigma(r)$.

In Backward Time-Stepping, the difference between measured and calculated scattered fields is utilized as a source to irradiate the original profile. The resulting adjoint fields denoted as $w_m\left(\rho; r, t\right)$ shall be utilized to compute the values of gradients and directions. Gradients and search directions are significant to updating the estimated reconstructed profiles in each iteration. Formulations of gradients $g_{\varepsilon_r}\left(r\right)$ and $g_\sigma\left(r\right)$ in conjugate gradient method are derived from Fréchet differential of cost function expressed in Eqs. (4) and (5), respectively.

$$g_{\varepsilon_r}\left(r\right) = 2\int_0^T \left(w_m\left(\rho; r, t\right) \frac{\partial \nu_m\left(\rho, r, t\right)}{\partial\left(ct\right)}\right) dt \tag{4}$$

$$g_\sigma\left(r\right) = 2\int_0^T w_m\left(\rho; r, t\right) \nu_m\left(\rho, r, t\right) dt \tag{5}$$

The term $w_m\left(\rho; r, t\right)$ is the adjoint fields due to the difference between measured and calculated signals exploited as a current source. Parameter c is the light speed of free space. Formulations in FBTS are solved with Finite-Difference Time-Domain (FDTD). Details of description on the FBTS algorithm can be referred in [15, 17, 18].

The segmentation is based on the research work by [19] in which Adaptive K-means clustering is employed to extract object's pixels from the original ROI. The AS-ROI process in FBTS is initiated at the Sth iteration which is determined based on empirical analyses. It must be ensured that the reconstructed profiles at the respective iteration for AS-ROI initiation have enough information on the object's size and location. Otherwise, the segmented region would not confine the sought object to be detected. In this research work, minimum clusters to be detected are three layers relative to free space, lung and tumour layers. The segmented region therefore should confine the tumour layer.

Providing that tumour layer has been distinguished, central coordinate (x_1, y_1) of object can be identified by using Eqs. (6) and (7).

$$x_1 = round\left(\frac{X_{\max} - X_{\min}}{2}\right) \tag{6}$$

$$y_1 = round\left(\frac{Y_{\max} - Y_{\min}}{2}\right) \tag{7}$$

Parameters $X_{\max}$ and $X_{\min}$ are maximum and minimum points that circumscribe the object layer in x direction. $Y_{\max}$ and $Y_{\max}$ on the other hands are maximum and minimum circumference points of y

direction. The distances in x and y directions with respect to the centre point of FDTD (x_0, y_0) are simply computed with Eqs. (8) and (9).

$$offsetX_{new} = x_1 - x_0 \tag{8}$$

$$offsetY_{new} = y_1 - y_0 \tag{9}$$

Size of the new reconstruction region that corresponds to object radius is determined by the maximum value obtained from Eq. (10) to (13). $radius_1$ to $radius_4$ are pointed to upper right, lower right, lower left and upper left directions, respectively, from the central coordinate (x_1, y_1) of a rectangle (formed by four points constitutes of $X_{\max}$, $X_{\min}$, $Y_{\max}$ and $Y_{\max}$) that circumscribes the detected object. Rationale of calculating radius in four directions is due to the inevitable occurrence of small error between these values during computation.

$$radius_1 = round\left(\sqrt{(X_{\max} - x_1)^2 + (Y_{\min} - y_1)^2}\right) \tag{10}$$

$$radius_2 = round\left(\sqrt{(X_{\max} - x_1)^2 + (Y_{\max} - y_1)^2}\right) \tag{11}$$

$$radius_3 = round\left(\sqrt{(X_{\min} - x_1)^2 + (Y_{\max} - y_1)^2}\right) \tag{12}$$

$$radius_4 = round\left(\sqrt{(X_{\min} - x_1)^2 + (Y_{\min} - y_1)^2}\right) \tag{13}$$

On the condition that the number of pixels in the new ROI exceeds or equal to the number of pixels in the initial ROI, the AS-ROI shall be repeated in the subsequent iteration of FBTS. Once the ROI is successfully rescaled down, then the optimization shall be reformulated as in Eq. (14).

$$F(\rho)' = \int_0^T \sum_{m=1}^{M} \sum_{n=1}^{N} K_{mn}(t) \left| V_m(\rho(r); r_n^r, t) - \tilde{V}_m(r_n^r, t) \right|^2 dt \tag{14}$$

Terms $\tilde{V}_m(r_n^r, t)$ and $V_m(\rho(r); r_n^r, t)$ in Eq. (14) are measured and calculated scattered fields computed in the new ROI.

2.2. AS-ROI with Iterative Edge Preserving Technique in FBTS

Edge preserving methods in this research work is implemented at the Rth iteration which is initiated after rescaling process. Edge preserving is implemented by means of regularization imposed on the solution and anisotropic diffusion applied to the reconstructed profiles. These edge preserving methods are alternately applied in even and odd iteration numbers.

At the Rth iteration, cost function is then reformulated into Eq. (15) which is the combination of rescaled FBTS and edge preserving regularization. The regularization function is given in Eq. (16).

$$F_{TOTAL}(\varepsilon_r, \sigma) = F(\varepsilon_r, \sigma)' + F_{EPR}(\varepsilon_r) \tag{15}$$

$$F_{EPR}(\varepsilon_r) = \lambda \iint_{\Omega} \varphi\left(\frac{\|\nabla \varepsilon_r\|}{\delta}\right) d\Omega \tag{16}$$

Note that in Eq. (15) only relative permittivity is considered to be regularized. This is to reduce the number of parameters involved for regularization since each profile needs individual parameter settings. λ in Eq. (16) represents regularization coefficient to balance the effect between FBTS and regularization. The term φ is the regularization function useful for diffusion for homogenous area confined within the detected edges. Image gradient denoted as $\|\nabla \varepsilon_r\|$ is computed by taking the summation of gradients in eight directions. Each gradient is calculated with finite difference across pixels. The term δ is the threshold parameter to distinguish edges and non-edges that define the area for diffusion. The term Ω refers to spatial domain of the new ROI.

The incorporation of regularization into the combined AS-ROI and FBTS result in total gradients of relative permittivity profile given in Eq. (17).

$$g_{\varepsilon_{rTOTAL}} = g_{\varepsilon_{rFBTS}} + g_{\varepsilon_{rEPR}} \tag{17}$$

Gradient of relative permittivity obtained from Fréchet differential of regularization cost functional is shown in Eq. (18).

$$g_{\varepsilon_{rEPR}} = -2\frac{\lambda}{\delta^2}\nabla \cdot (b_a \nabla \varepsilon_{ra} + b_b \nabla \varepsilon_{rb}) \tag{18}$$

Parameters b_a and b_b given in Eqs. (19) and (20) are weighting functions in vertical and diagonal directions which are approximately zero in the availability of edges. $\nabla\varepsilon_{ra}$ and $\nabla\varepsilon_{rb}$ are image gradients in vertical and diagonal directions, respectively.

$$b_a = 1/\left(1 + (\nabla\varepsilon_{ra}/\delta)^2\right)^2 \tag{19}$$

$$b_b = 1/\left(2\left(1 + (\nabla\varepsilon_{rb}/\delta)^2\right)^2\right) \tag{20}$$

In odd iteration number, anisotropic diffusion is implemented on the nonregularized relative permittivity given in Eq. (21).

$$\frac{\partial\varepsilon_r(x,y,t_{AD})}{\partial t_{AD}} = \operatorname{div}\left[g\left(\|\nabla\varepsilon_r(x,y,t_{AD})\|\right)\cdot\nabla\varepsilon_r(x,y,t_{AD})\right] \tag{21}$$

$$g\left(\|\nabla\varepsilon_r(x,y,t_{AD})\|\right) = 1/\left(1 + (\nabla\varepsilon_r/\delta)^2\right) \tag{22}$$

Diffusivity function $g\left(\|\nabla\varepsilon_r(x,y,t_{AD})\|\right)$ in Eq. (22) is comparable to weighting function applied in regularization. Nevertheless, the diffusivity function in anisotropic diffusion is commonly defined to be Hebert and Leahy regularization function [28]. Variable t_{AD} denotes the time evolution for the filter. In this research work, convergence criterion for t_{AD} is defined as 1 to avoid over smoothing effect since it is implemented in every alternate iteration after rescaling process. Further explanation on anisotropic diffusion algorithm can be found in [29, 30].

3. RESULTS AND DISCUSSION

Three lung models are considered for the first analysis in which size and object profiles are varied. The phantom models are plotted based on transverse CT scan of thoracic wall taken from the Cancer Imaging Archive (TCIA) Public Access [31]. Lungs area is manually segmented from the image. Dielectric profiles are computed based on the literature and Cole-Cole expression dataset at 2 GHz frequency by Gabriel, C [32]. The first model, namely Model #1, consists of 8087 pixels. Model #2 and Model #3 comprise 9135 pixels. Lung profiles for all models are computed based on best case capacity ratio of healthy lungs, consists of 66% air, 14% blood and 20% parenchyma [33]. Profiles values of parenchyma are determined based on the average value of inflated and deflated lungs [34].

Mediastinum area is regarded as an object under test (OUT) in Model #1. The profiles are directly taken after heart muscle profiles. Tumour in Model #2 is computed based on proportion of 60% blood, 20% muscle and 20% of blood vessel [35]. The composition of tumour in Model #3 is computed by using the middle range of minimum and maximum proportion of cancerous lungs tissues with respect to healthy lungs [36]. The computed dielectric profile settings for each model are summarized as in Table 1. Proper profile values to be assigned as the initial guess are necessary to govern the optimization process to correct solution. Optimal initial guess values in this research work were empirically chosen for each tested model.

Table 1. Dielectric profiles setting.

Layer	Model #1		Model #2		Model #3	
	ε_r	$\sigma\left(\mathrm{Sm}^{-1}\right)$	ε_r	$\sigma\left(\mathrm{Sm}^{-1}\right)$	ε_r	$\sigma\left(\mathrm{Sm}^{-1}\right)$
Layer 1 (OUT)	55.80	1.91	54.68	1.84	33.41	0.92
Layer 2 (Lung)	15.91	0.51	15.91	0.51	15.91	0.51
Layer 3 (Free space)	1.00	0.00	1.00	0.00	1.00	0.00

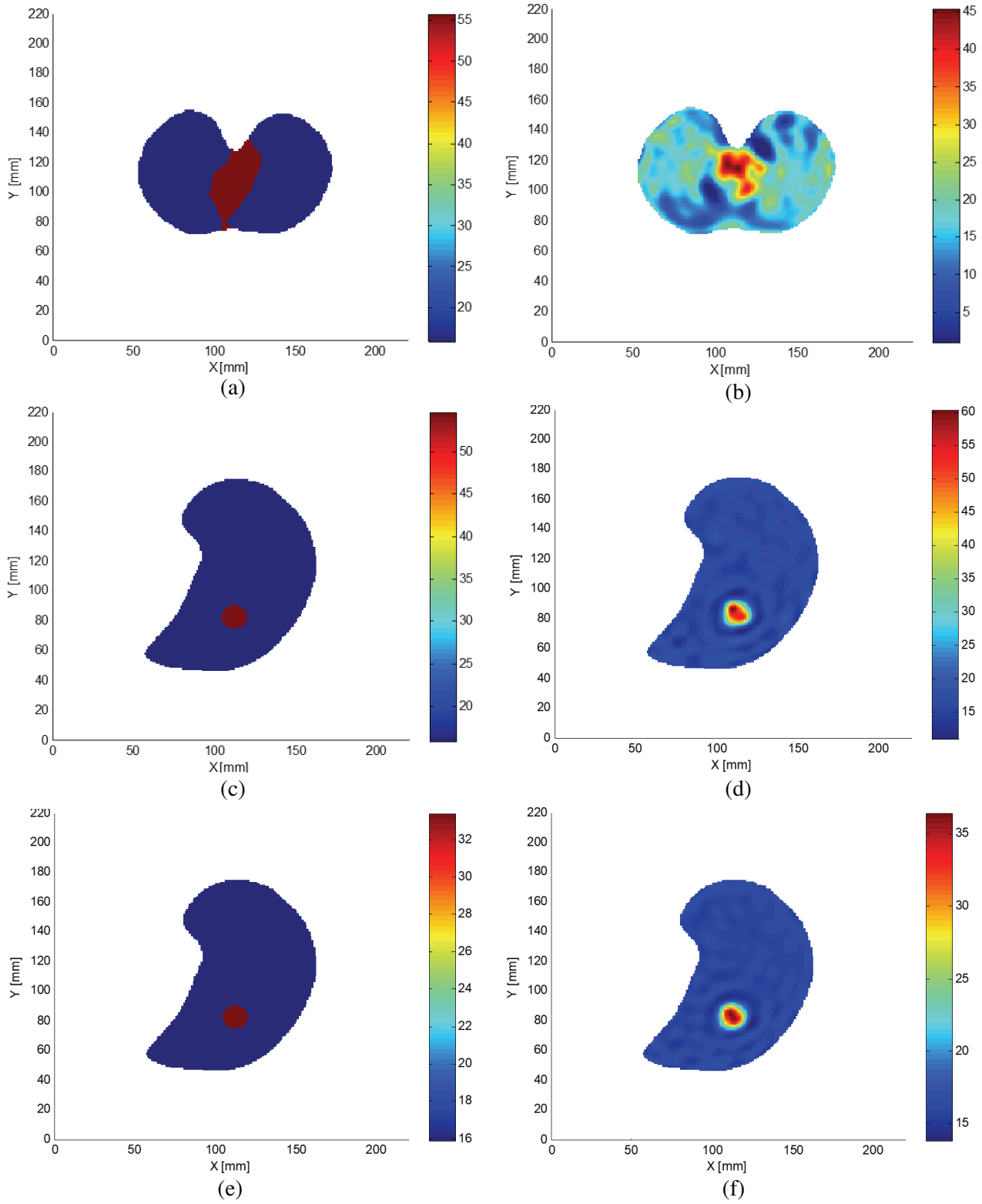

Figure 2. a) Actual image of Model #1. (b) Reconstructed image of Model #1. (c) Actual image of Model #2. (d) Reconstructed image of Model #2. (e) Actual image of Model #3. (f) Reconstructed image of Model #3.

A tumour as an OUT is embedded in the original ROI of lung. Free space is utilized as a coupling medium. Antennas are evenly spaced from each other in 85 mm radius irradiating modulated Gaussian pulse with centre frequency of 2 GHz and bandwidth of 1.3 GHz. Fields' scattering processes are simulated on a FDTD lattice with solution space of $190 \times 190\,\text{mm}^2$ and cell size of $1\,\text{mm}^2$. The solution space is delimited by Convolutional Perfectly Matched Layer (CPML) of 15 mm thickness as an absorbing boundary condition (ABC). Convergence criterion for the whole inversion process is 100 iterations.

The value of R to initiate regularization process and all parameters related to regularization and anisotropic diffusion are based on heuristic analyses. Suitable parameters were determined based on the accuracy of reconstructed profiles. Quality of reconstructed profiles was evaluated by using Mean Squared Error (MSE) metric as an indicator. Optimal accuracy value was found by utilizing Geman and McCLure regularization function [37] with regularization coefficient of 5.0×10^{-10} and threshold parameter of 1.25. As for the anisotropic diffusion, optimal diffusion conductivity speed is 0.1 which has a similar function to regularization coefficient. The threshold parameter for anisotropic diffusion has a similar setting to the regularization process.

Relative permittivities of actual and reconstructed profiles by FBTS for each phantom model are shown in Figure 2. Among the three tested models, it was obviously seen that Model #1 in Figure 2(b) was poorly reconstructed with prominently high MSE level at 172.049. The peripheral object and location were unable to be distinguished from lungs' layer. Model #2 with a smaller object area

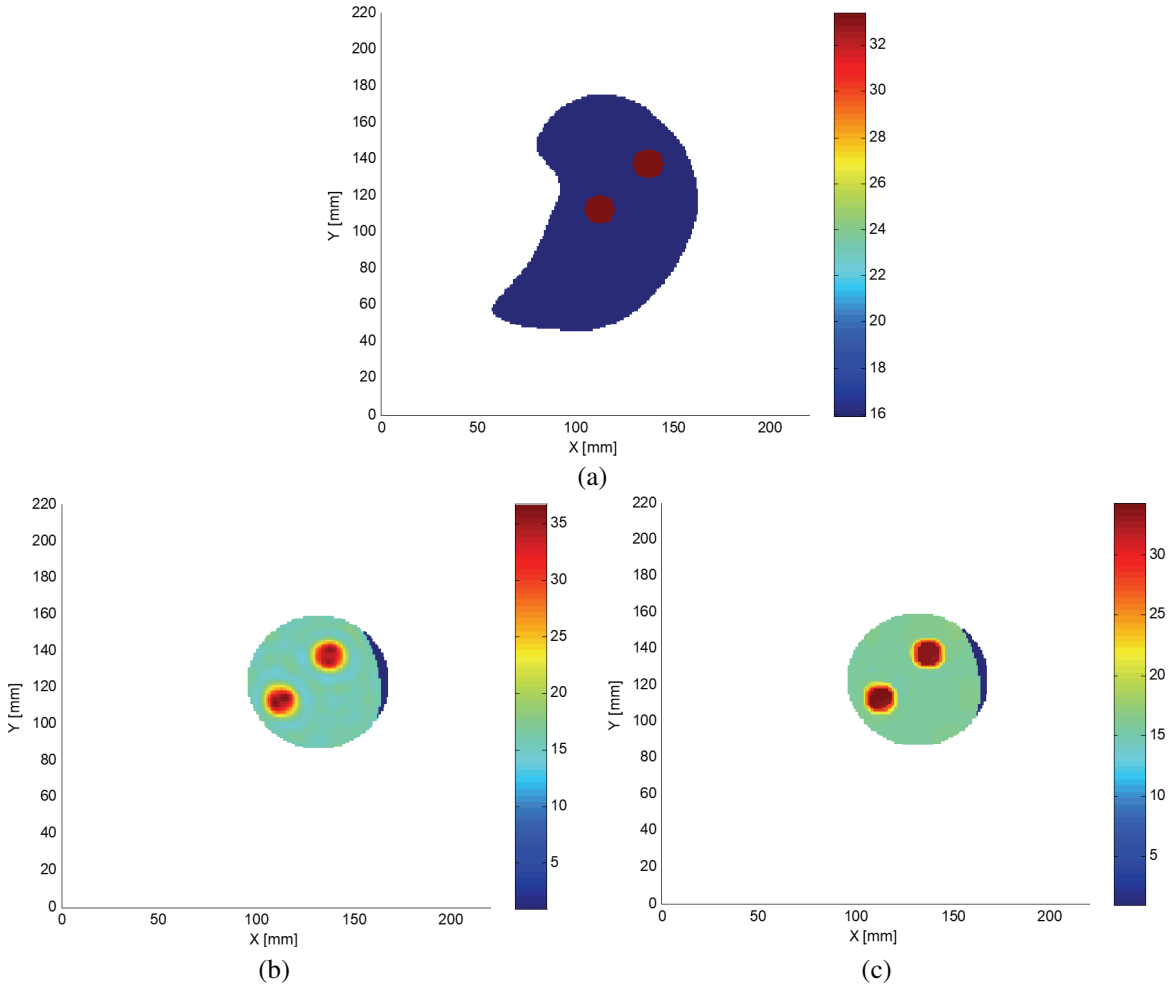

Figure 3. Cross sectional top view in x-y plane of (a) actual object (b) AS-ROI in FBTS (c) AS-ROI in the regularized FBTS.

attained reasonable MSE level of 6.917, illustrated in Figure 2(d). Model #3 with reduced contrast level compared to Model #2 had better accuracy level at 1.147, shown in Figure 2(f). The embedded objects for both Models #2 and #3 were notable in their shape, size and location. Based on the accuracy level, Model #3 was utilized for later analysis.

Cross sectional top view of relative permittivity distributions of two embedded tumours are illustrated in Figure 3. It shows comparison between the actual phantom model and reconstructed profile by AS-ROI in FBTS along with the combined method of AS-ROI and edge preserving techniques in FBTS. Note that in Figure 3(b), AS-ROI method has successfully reduced the reconstruction region analogous to the tumours geometrical configuration. The regularized version as shown in Figure 3(c) has eliminated visible ring artifacts in the reconstructed image generated by the combined AS-ROI and FBTS in Figure 3(b).

The elimination of artifacts can be clearly seen from cross sectional side view for each tumour shown in Figure 4 and Figure 5. In Figure 4(a) and Figure 5(a), it is shown that AS-ROI had assisted

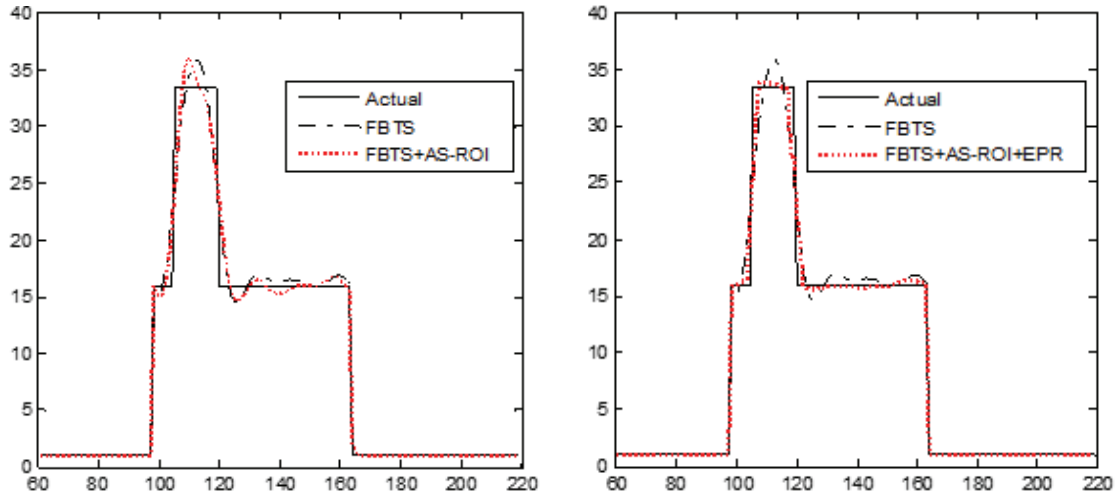

Figure 4. Cross sectional side view of object #1 which offset at $(0, 0)$ from centre coordinate in Model #3 utilizes (a) AS-ROI in FBTS (b) AS-ROI in the regularized FBTS.

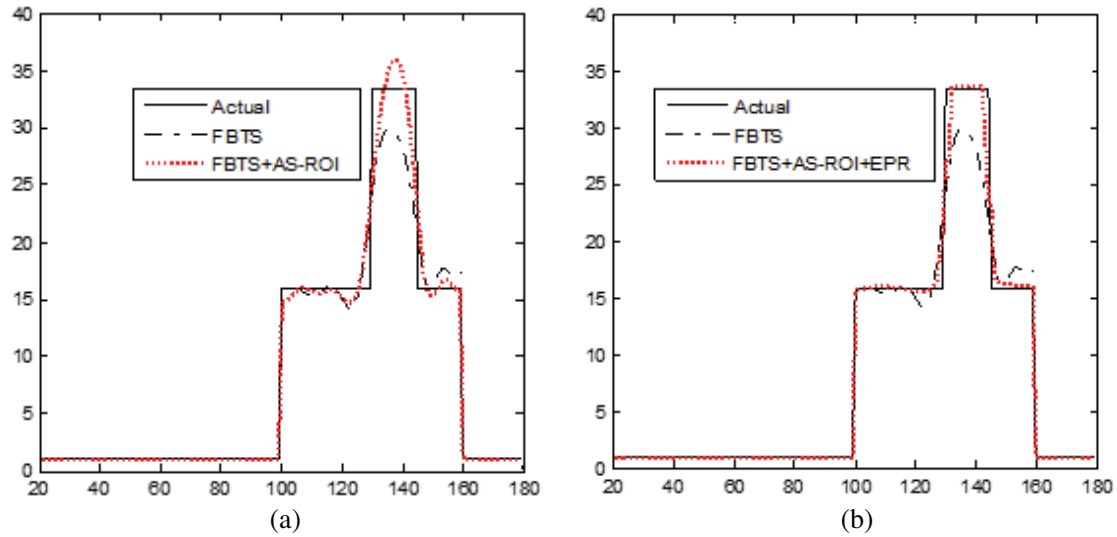

Figure 5. Cross sectional side view of object #2 which offset at (25, 25) from centre coordinate in Model #3 utilizes (a) AS-ROI in FBTS (b) AS-ROI in the regularized FBTS.

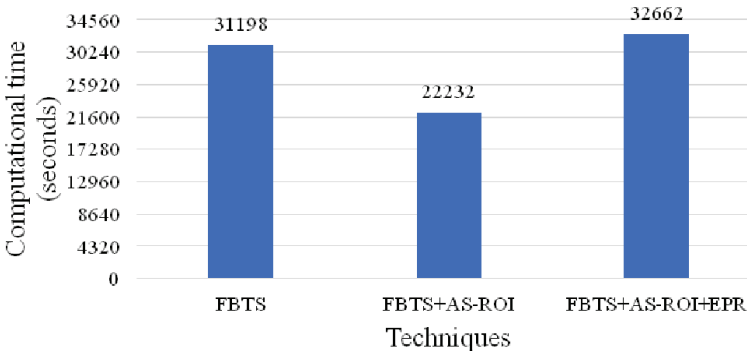

Figure 6. Computational efficiency measure.

the optimization solution to reach approximate profiles' distribution with respect to the actual profiles which is particularly obvious in Figure 5(a). However, there are fluctuations along the peripheral side view that may appear as ring artifacts in the top view. These fluctuations are greatly reduced in Figure 4(b) and Figure 5(b) with the incorporation of regularization into the combined AS-ROI and FBTS.

In terms of MSE level, the reconstructed profile by FBTS attained an accuracy of 5.229. The implementation of AS-ROI in FBTS attained MSE of 3.913 which is equivalent to 25.617% increment with respect to the FBTS. The regularized version further elevates the precision level to 3.102 or contributes to 40.667% of increment. The accuracy difference between the regularized and non-regularized cases of AS-ROI in FBTS was 15.050%.

Figure 6 shows comparison in computational time among FBTS, AS-ROI in FBTS and AS-ROI in the regularized FBTS. The reduction number of pixels with the implementation of AS-ROI in FBTS had reduced the computational time about 28.74% compared to FBTS. Integrating edge preserving technique into AS-ROI in FBTS however had consumed an additional time about 4.69%. Nevertheless, it is a major tradeoff between accuracy and computational time which is similar to filtered FBTS in [21]. In order to achieve the same accuracy level as the latter technique, both FBTS and AS-ROI in FBTS require additional antennas or iteration numbers for convergence. Therefore, computational time of both techniques will also increase since time is proportional to the number of antennas and iterations of optimization.

4. CONCLUSIONS

It was shown in the first analysis that accuracy in the profiles' distribution increased with the reduced object size and contrast level between layers. High contrast is essential to distinguishing layers of an unknown problem. However, too high contrast values can overwhelm the scattering fields process which results in false solutions in the profile reconstruction. AS-ROI has been proven effective to locate and estimate object's size based on priori data obtained from FBTS. Despite operating at the same resolution level as the FBTS, the combined AS-ROI with FBTS method had successfully elevated the accuracy of the dielectric profile distribution. Edge preserving technique which is an alternate method of edge preserving regularization and anisotropic diffusion had boosted the precision to even higher level. However, computational time had increased with the implementation of the edge preserving technique into AS-ROI. Multi-resolution approach in AS-ROI method shall be considered for future works in which exterior pixels outside object region shall also be taken into analyses. Edge operator along with the increased number of gradients involved are among interesting topics to explore its effect towards the sensitivity of regularization in FBTS.

ACKNOWLEDGMENT

The authors acknowledge the financial support rendered by Universiti Malaysia Sarawak (UNIMAS) through Fundamental Research Grant Scheme — FRGS/1/2015/TK04/UNIMAS/02/1, Ministry of Higher Education, Malaysia.

REFERENCES

1. Moriyama, T., G. Oliveri, M. Salucci, and T. Takenaka, "A multi-scaling forward-backward time-stepping method for microwave imaging," *IEICE Electronics Express*, Vol. 11, No. 16, 1–12, 2014.
2. Chen, X., K. Xu, F. Shen, L. Ran, and Y. Zhong, "Subspace-based optimization method coupled with multiplicative regularization for edge-preserving inversion," *Antennas and Propagation & USNC/URSI National Radio Science Meeting, 2015 IEEE International Symposium*, 898–899, 2015.
3. Zhong, Y., M. Lambert, D. Lesselier, and X. Chen, "A new integral equation method to solve highly nonlinear inverse scattering problems," *IEEE Transactions on Antennas and Propagation*, Vol. 64, No. 5, 1788–1799, 2016.
4. Garcia-Fernandez, M., C. Garcia, Y. Alvarez, and F. Las-Heras, "Influence of contour smoothness and electric size on the profile reconstruction of metallic objects using hybrid optimization," *EUROCON 2015-International Conference on Computer as a Tool (EUROCON), IEEE*, 1–6, 2015.
5. Moriyama, T., M. Salucci, T. Tanaka, and T. Takenaka, "Image reconstruction from total electric field data with no information on incident field," *Journal of Electromagnetic Waves and Applications*, Vol. 30, No. 9, 1162–1170, 2016.
6. Rekanos, I. T., "Shape reconstruction of a perfectly conducting scatterer using differential evolution and particle swarm optimization," *IEEE Transactions on Geoscience and Remote Sensing*, Vol. 46, No. 7, 1967–1974, 2008.
7. Scapaticci, R., O. M. Bucci, I. Catapano, and L. Crocco, "Differential microwave imaging for brain stroke followup," *International Journal of Antennas and Propagation*, Vol. 2014, 2014.
8. Gantala, G., C. V. Krishnamurthy, and K. Balasubramaniam, "Location and sizing of defects in coated metallic pipes using limited view scattered data in frequency domain," *Journal of Nondestructive Evaluation*, Vol. 35, No. 2, 1–13, 2016.
9. Zamani, A., S. A. Rezaeieh, and A. M. Abbosh, "Lung cancer detection using frequency-domain microwave imaging," *Electronics Letters*, Vol. 51, No. 10, 740–741, 2015.
10. Hidayetoğlu, M., C. Yang, L. Wang, A. Podkowa, M. Oelze, W. M. Hwu, and W. C. Chew, "Parallel solutions of inverse multiple scattering problems with born-type fast solvers," *2016 Progress In Electromagnetic Research Symposium (PIERS)*, 916–920, Shanghai, China, Aug. 8–11, 2016.
11. Bao, G., P. Li, J. Lin, and F. Triki, "Inverse scattering problems with multi-frequencies," *Inverse Problems*, Vol. 31, No. 9, 93001, 2015.
12. Poli, L., G. Oliveri, P. P. Ding, T. Moriyama, and A. Massa, "Multifrequency bayesian compressive sensing methods for microwave imaging," *JOSA A*, Vol. 31, No. 11, 2415–2428, 2014.
13. Salucci, M., L. Tenuti, C. Nardin, M. Carlin, F. Viani, G. Oliveri, and A. Massa, "GPR survey through a multi-resolution deterministic approach," *Antennas and Propagation Society International Symposium (APSURSI)*, IEEE, Vol. 2014, 882–883, 2014.
14. Salucci, M., L. Poli, N. Anselmi, and A. Massa, "Multifrequency particle swarm optimization for enhanced multiresolution GPR microwave imaging," *IEEE Transactions on Geoscience and Remote Sensing*, Vol. 55, No. 3, 1305–1317, 2016.
15. Moriyama, T., G. Oliveri, A. Massa, and T. Takenaka, "Iterative multiscaling strategy incorporated into time domain inverse scattering method for cross-borehole imaging," *Geoscience and Remote Sensing Symposium (IGARSS), 2011 IEEE International*, No. 1, 846–849, 2011.
16. Moriyama, T., M. Salucci, G. Oliveri, L. Tenuti, P. Rocca, and A. Massa, "Multi-scaling deterministic imaging for GPR survey," *Antenna Measurements & Applications (CAMA), 2014 IEEE Conference*, 1–3, 2014.
17. Rocca, P., M. Benedetti, M. Donelli, D. Franceschini, and A. Massa, "Evolutionary optimization as applied to inverse scattering problems," *Inverse Problems*, Vol. 25, No. 12, 123003, 2009.
18. Juliana, N., S. Shafrida, and K. A. H. Ping, "Automated scaling region of interest (AS-ROI) in inverse scattering method for tomographic image reconstruction," *2017 Progress In Electromagnetics Research Symposium — Fall (PIERS — FALL)*, 1648–1653, Singapore, Nov. 19–22, 2017.

19. Guang, Y., K. A. H. Ping, A. S. C. Chie, N. S. Wei, and M. Thelaha, "Preliminary study of forward-backward time-stepping technique with edge-preserving regularization for object detection applications," *BioSignal Analysis, Processing and Systems (ICBAPS), 2015 International Conference*, 77–81, 2015.
20. Yong, G., K. A. H. Ping, S. Shafrida, M. Mohamad Hamiruce, S. Mohd Iqbal, T. Moriyama, and T. Takenaka, "Profile reconstruction utilizing forward-backward time-stepping with the integration of automated edge-preserving regularization technique for object detection applications," *Progress In Electromagnetics Research M*, Vol. 54, 125–135, 2017.
21. Juliana, N., S. Shafrida, K. A. H. Ping, A. M. Dayang Azra, and A. Z. Dyg Norkhairunnisa, "Iterative refinement in inverse scattering technique with median filter," *Applied Electromagnetics (APACE), 2016 IEEE Asia-Pacific Conference*, 62–67, 2016.
22. Ping, K. A. H., T. Moriyama, T. Takenaka, and T. Tanaka, "Two-dimensional forward-backward time-stepping approach for tumor detection in dispersive breast tissues," *Microwave Symposium (MMS), 2009 Mediterranean*, 2009.
23. Takenaka, T., T. Moriyama, K. A. H. Ping, and T. Yamasaki, "Microwave breast imaging by the filtered forward-backward time-stepping method," *Electromagnetic Theory (EMTS), 2010 URSI International Symposium*, 946–949, 2010.
24. Johnson, J. E., T. Takenaka, K. A. H. Ping, S. Honda, and T. Tanaka, "Advances in the 3-D forward-backward time-stepping (FBTS) inverse scattering technique for breast cancer detection," *IEEE Transactions on Biomedical Engineering*, Vol. 56, No. 9, 2232–2243, 2009.
25. Elizabeth, M. A. P., K. A. H. Ping, N. S. Wei, W. Z. A. Wan Azlan, M. Thelaha, O. Al-Khalid, T. Moriyama, and T. Takenaka, "2-D reconstruction of breast image using forward-backward time-stepping method for breast tumour detection," *Applied Electromagnetics (APACE), 2012 IEEE Asia-Pacific Conference*, 70–73, 2012.
26. Elizabeth, M. A. P., K. A. H. Ping, R. Nordiana, and T. Moriyama, "Chebyshev filter applied to an inversion technique for breast tumour detection," *International Journal of Research in Engineering & Technology*, Vol. 4, No. 6, 210–218, 2015.
27. Chie, A. S. C., Y. Guang, K. A. H. Ping, N. S. Wei, and R. Nordiana, "Preliminary results of integrating Tikhonov's regularization in forward-backward time-stepping technique for object detection," *Applied Mechanics and Materials*, Vol. 833, 170–175, 2016.
28. Hebert, T. and R. Leahy, "A generalized EM algorithm for 3-D bayesian reconstruction from poisson data using gibbs priors," *IEEE Transactions on Medical Imaging*, Vol. 8, No. 2, 194–202, 1989.
29. Fada, G., T. Phuc, G. Shuaiping, and Z. Lina, "Anisotropic diffusion filtering for ultrasound speckle reduction," *Science China Technological Sciences*, Vol. 57, No. 3, 607–614, 2014.
30. Mithun Kumar P. K., M. G. Arefin, M. Motiur Rahman, and A. S. M. Delowar Hossain, "Automatically gradient threshold estimation of anisotropic diffusion for Meyer's watershed algorithm based optimal segmentation," *International Journal of Image, Graphics and Signal Processing*, Vol. 6, No. 12, 26–31, 2014.
31. Grove, O., A. E. Berglund, M. B. Schabath, H. J. Aerts, A. Dekker, H. Wang, and R. J. Gillies, "Quantitative computed tomographic descriptors associate tumor shape complexity and intratumor heterogeneity with prognosis in lung adenocarcinoma," *PloS one*, Vol. 10, No. 3, 2015.
32. Anderson, V. and J. Rowley, "Tissue dielectric properties calculator," *Clayton, Victoria, Australia: Telstra Research Laboratories*, 1998.
33. Holman, B. F., V. Cuplov, L. Millner, B. F. Hutton, T. M. Maher, A. M. Groves, and K. Thielemans, "Improved correction for the tissue fraction effect in lung PET/CT imaging," *Physics in Medicine and Biology*, Vol. 60, No. 18, 7387–7402, 2015.
34. Hartsgrove, G., A. Kraszewski, and A. Surowiec, "Simulated biological materials for electromagnetic radiation absorption studies," *Bioelectromagnetics*, Vol. 8, No. 1, 29–36, 1987.
35. Babarinde, O. J., M. F. Jamlos, P. J. Soh, D. M. M. P. Schreurs, and A. Beyer, "Microwave imaging technique for lung tumour detection," *Microwave Conference (GeMiC), 2016 German*, 100–103, 2016.

36. Wang, J. R., B. Y. Sun, H. X. Wang, S. Pang, X. Xu, and Q. Sun, "Experimental study of dielectric properties of human lung tissue in vitro," *Journal of Medical and Biological Engineering*, Vol. 34, No. 6, 598–604, 2014.
37. Charbonnier, P., L. Blanc-Féaud, G. Aubert, and M. Barlaud, "Deterministic edge-preserving regularization in computed imaging," *IEEE Transactions on Image Processing*, Vol. 6, No. 2, 298–311, 1997.